Single-Photon Diode by Exploiting the Photon Polarization in a Waveguide

Yuecheng Shen (沈乐成),[1] Matthew Bradford,[1] and Jung-Tsung Shen (沈榮聰)[1,2,*]

[1]Department of Electrical and Systems Engineering, Washington University in St. Louis, St. Louis, Missouri 63130, USA
[2]Center for Materials Innovation, Washington University in St. Louis, St. Louis, Missouri 63130, USA

(Received 28 May 2011; published 17 October 2011)

A single-photon optical diode operates on individual photons and allows unidirectional propagation of photons. By exploiting the unique polarization configuration in a waveguide, we show here that a single-photon optical diode can be accomplished by coupling a quantum impurity to a passive, linear optical waveguide which possesses a locally planar, circular polarization. We further show that the diode provides a near unitary contrast for an input pulse with finite frequency bandwidth and can be implemented in a variety of types of waveguides. Moreover, the performance of the diode is not sensitive to the intrinsic dissipation of the quantum impurity.

DOI: 10.1103/PhysRevLett.107.173902 PACS numbers: 42.82.Et, 42.50.−p, 42.70.Qs

Complete optical signal isolation is critical for integrated nanophotonics [1]. Recent advances in solid-state single-photon sources [2–5] and nanoscale fabrication make on-chip quantum optics and information processing attainable. To ensure proper operations of the quantum optical devices, parasitic reflections between optical devices must be completely suppressed at the single-photon level, as such feedback can have deleterious effects on the operation of optical devices based on interferometric designs. An optical diode is a spatially nonreciprocal device which allows unidirectional propagation of a signal, acting as an optical isolator at a given wavelength [6]. In an ideal case, its transmission is 100% in the "forward" direction ($T_f = 1$), while it vanishes for the "backward" direction ($T_b = 0$), yielding a unitary contrast $\eta \equiv (T_f - T_b)/(T_f + T_b) = 1$. Various possible solid-state optical diodes have been proposed or demonstrated, from standard bulk Faraday rotators (due to small Verdet constant, the Faraday rotators are typically of centimeter size [7,8]), to thin film devices based on magneto-optic effects in a Mach-Zehnder geometry at centimeter scale [9], use of a graded gain medium with a 10 cm long glass capillary filled with ethanol [10], and approaches that tailor the nonlinear responses which require certain optical power so that the nonlinearity manifests [6,11]. With the capability of controlling light-matter interactions in ultralow power regimes and down to single-photon levels [12,13], it is also desirable to achieve optical signal isolation at the single-photon level at sub-μm chip scale for integrated nanophotonics. In this Letter, we show that near complete optical isolation can be achieved at the single-photon level by coupling a quantum impurity to a passive, linear waveguide which has a locally planar, circular polarization. Such a configuration does not rely upon the use of bulk nonlinear materials or quasiphase matching, and can be implemented in various types of waveguides.

We start by describing the configuration of the single-photon diode. The diode is accomplished by coupling a quantum impurity to a passive, linear waveguide [Fig. 1(a)]. The waveguide is a single-polarization single-mode (SPSM) waveguide, with a planar and circular polarization at the location of the impurity at a fixed frequency (the operating frequency). The circularly polarized state reverses its orientation for opposite wave vectors [Fig. 1(b)], due to time-reversal symmetry. We will take the polarization plane as the x-y plane. With an external dc magnetic field $\mathbf{B}$ in the z direction that breaks the time-reversal symmetry, the energy levels of the impurity are Zeeman split and each level couples to one circularly polarized state [Fig. 1(c)]. The design strategies and rigorous conditions for SPSM waveguides have been discussed before [14]; numerically, we found that a locally planar circular polarization can be achieved for a variety of waveguides, as will be shown below. The impurity can be a quantum dot [15–17] or an atom doped in semiconductors [18–20]. The transition frequencies of different quantum

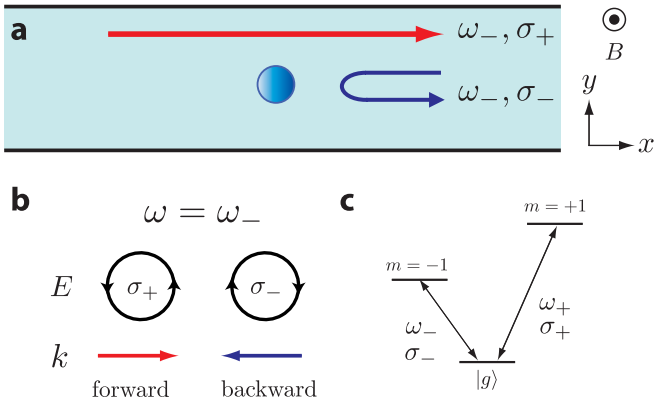

FIG. 1 (color online). Schematics of the single-photon diode. (a) A quantum impurity (blue dot) is coupled to a passive, linear SPSM waveguide. (b) At the operating frequency, the waveguide possesses a locally planar circular polarization. The polarization reverses its orientation for opposite wave vectors. (c) The energy level diagram with the presence of an external magnetic field.

impurities cover a wide range from microwave to far infrared.

We note that in this configuration the wave vector $\mathbf{k}$ is perpendicular to the magnetic field $\mathbf{B}$, which is the same as in the Voigt (transverse) configuration and is different from the Faraday (longitudinal) configuration [21] wherein $\mathbf{k}$ is parallel to $\mathbf{B}$. Moreover, the wave vector and the polarization lie in the same plane that is perpendicular to the magnetic field. Such a unique configuration is possible only in a confined geometry, such as a waveguide. When coupled to a dipole, the interaction between the dipole and the photon field is given by

$$\begin{aligned} H_I &= -\mathbf{d}\cdot\mathbf{E} \\ &= -\left(\frac{d_x + id_y}{\sqrt{2}}\frac{E_x - iE_y}{\sqrt{2}} + \frac{d_x - id_y}{\sqrt{2}}\frac{E_x + iE_y}{\sqrt{2}} + d_z E_z\right) \\ &\equiv -(d_+ E_+ + d_- E_- + d_z E_z), \end{aligned} \tag{1}$$

where the in-plane electric field is decomposed into a linear combination of left- and right-hand circular components as $E_x\hat{\mathbf{x}} + E_y\hat{\mathbf{y}} = E_+\hat{\boldsymbol{\sigma}}_+ + E_-\hat{\boldsymbol{\sigma}}_-$ [here $\hat{\boldsymbol{\sigma}}_\pm = (\hat{\mathbf{x}} \pm i\hat{\mathbf{y}})/\sqrt{2}$ corresponds to the left- and right-hand circular polarization unit vectors [22]]. In the case of electric or magnetic $\Delta m = \pm 1$ dipole transitions, the impurity interacts only with the circularly polarized photon modes $\sigma_\pm$ [Fig. 1(c)]. The selection rules state that the $\Delta m = 1$ transition couples to σ_+ polarization and only d_+ has nonzero matrix elements, while the $\Delta m = -1$ transition couples to σ_- polarization and only d_- has nonzero matrix elements. For dipole transition with transition frequency ω_d, the transmission and reflection amplitudes of the photon at frequency ω are given by $t(\omega) = (\omega - \omega_d + i\gamma)/(\omega - \omega_d + i\Gamma + i\gamma)$ and $r(\omega) = i\Gamma/(\omega - \omega_d + i\Gamma + i\gamma)$, where Γ is the external linewidth of the dipole due to waveguide-quantum dot coupling, and γ is the intrinsic dissipation rate of the quantum dot [23,24]. The transmission and reflection coefficients are given by $T(\omega) = |t(\omega)|^2$ and $R(\omega) = |r(\omega)|^2$.

We now describe the operating scheme for achieving the photonic rectification: For a photon entering from the left (the "forward" direction) with frequency ω_-, since the photon mode is σ_+ polarized at the location of the impurity, the photon couples only to the $m = 1$ atomic state that has a transition frequency ω_+; for a large frequency mismatch ($\omega_+ - \omega_- \gg$ the frequency bandwidth of the pulse), the photon will not interact appreciably with the impurity and has a perfect transmission ($T_f = 1$). On the other hand, when the photon enters from the right (the "backward" direction) with frequency ω_-, since the photon mode is σ_- polarized at the location of the impurity, the photon interacts resonantly with the $m = -1$ atomic state, giving rise to a zero transmission ($T_b = 0$) [23] and thus yields a unitary contrast. We emphasize that the polarization of the waveguide mode at frequency ω_+ is not important for the operation. Alternatively, the photonic rectification can be achieved at frequency ω_+ when the waveguide is designed to have a locally planar, circular polarization at ω_+. In this case, the forward and backward directions are reversed: photons entering from the right are now perfectly transmitted, while photons incident from the left are completely reflected.

Having introduced the device configuration and the basics of the operating scheme, we now present designs of SPSM waveguides that possess locally planar circular polarization. The first example is a two-dimensional (uniform in the z direction) line defect waveguide in silicon (dielectric constant $\epsilon = 13$), formed by removing a row of air columns from an otherwise perfect triangular lattice of air columns [Fig. 2(a)]. Such a system is known for having a broad complete photonic band gap for both transverse electric (TE) (electric field in the x-y plane) and transverse magnetic (TM) (magnetic field in the x-y plane) modes [25]. Figure 2(b) plots the band structure of the line defect

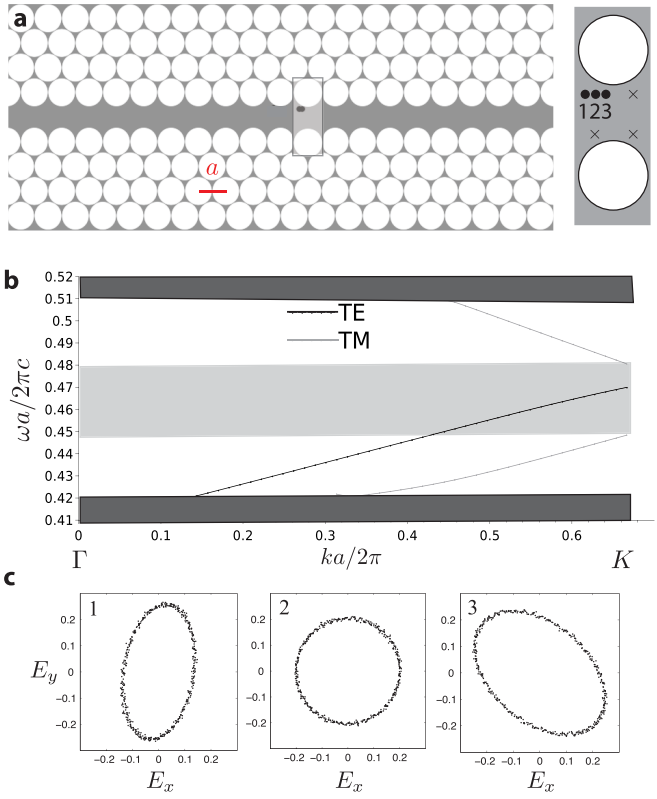

FIG. 2 (color online). Schematics and polarization states of a line defect waveguide. (a) A line defect waveguide in silicon ($\epsilon = 13$) with triangular lattice of air columns. A unit cell (along the x direction) of the waveguide is shown on the right. (b) The band structure of the waveguide. In the frequency range from 0.45 ($2\pi c/a$) to 0.47 ($2\pi c/a$), only TE mode exists and the waveguide is a SPSM waveguide. (c) The polarizations at three representative points [shown by black dots in (a)] at $\omega = 0.46$ ($2\pi c/a$). The polarization can be expressed in the form $a_x\cos(\omega t + \phi_x)\hat{\mathbf{x}} + a_y\cos(\omega t + \phi_y)\hat{\mathbf{y}}$. For point 2, the relative deviations for $|\Delta a/a_x|$ and $|\Delta\phi/(\pi/2)|$ are 1.3% and 1.4%, respectively.

waveguide along the Γ-K direction, which exhibits a complete band gap extending from 0.42 ($2\pi c/a$) to 0.51 ($2\pi c/a$). In particular, from the frequency range 0.45 ($2\pi c/a$) to 0.47 ($2\pi c/a$), the waveguide is a SPSM waveguide as only TE mode exists.

The line defect waveguide has discrete translational symmetry along the waveguide; the polarization pattern thus is periodic in the x direction with a periodicity a. To investigate the spatial variation of the polarization within a unit cell [Fig. 2(a) right), we scan through a horizontal line which locates at a distance $0.546a$ from the center of the closest air hole. Figure 2(c) plots the polarizations at three representative points within the unit cell which are located at a distance from the left edge of the unit cell $0.15a$, $0.23a$, and $0.30a$, respectively, at frequency $\omega = 0.46\ (2\pi c/a)$. The polarization at point 2 is found numerically to be circular. Moreover, we have numerically confirmed that only four points within the unit cell possess circular polarization: Besides point 2, the other three points [indicated by $\times$ in Fig. 2(a)] are obtained through mirror symmetry with respect to the center of the unit cell.

A practical diode must be able to operate over a finite frequency bandwidth. For a photon pulse with a finite frequency bandwidth, at detuned frequencies $\omega \neq \omega_-$ (the operating frequency), there are two possible predominant degrading factors to the performance of the diode: (1) the polarization becomes elliptic; an elliptic polarization is a linear superposition of both σ_+ and σ_- states, and thus couples to *both* transitions $\Delta m = \pm 1$; and (2) imperfect transmissions in both directions [23] [i.e., $T_f(\omega) \neq 1$ and $T_b(\omega) \neq 0$] at off-resonant frequencies $\omega \neq \omega_-$. Here we examine these issues and show that complete photonic rectification can still be achieved for a photon pulse. In general, for an incoming pulse $\phi(x, t)$ propagating in a waveguide with wave form $\phi(x, t) = \int d\omega g(\omega) e^{ik(\omega)x - i\omega t}$, the *pulse* transmission T and reflection R are generalizations of abovementioned $T(\omega)$ and $R(\omega)$; in this case, one needs to take into account the Fourier component $g(\omega)$ of the pulse, as well as the waveguide mode polarization. T and R are given by

$$T = \frac{\int d\omega \{u^2(\omega)|g(\omega)t_+(\omega)|^2 + v^2(\omega)|g(\omega)t_-(\omega)|^2\}}{\int d\omega |g(\omega)|^2}, \tag{2}$$

$$R = \frac{\int d\omega \{u^2(\omega)|g(\omega)r_+(\omega)|^2 + v^2(\omega)|g(\omega)r_-(\omega)|^2\}}{\int d\omega |g(\omega)|^2}, \tag{3}$$

where $t_\pm(\omega)$ and $r_\pm(\omega)$ are the transmission and reflection amplitudes at frequency ω for the $\Delta m = \pm 1$ transitions, respectively (i.e., $\omega_d = \omega_\pm$). $u(\omega)$ and $v(\omega)$ are real numbers which describe the ellipticity of the polarization in the waveguide as a function of frequency: The polarization at frequency ω is decomposed as $u(\omega)\hat{\sigma}_+ + v(\omega)\hat{\sigma}_-$. [$\hat{\sigma}_\pm = (\hat{\mathbf{x}} \pm i\hat{\mathbf{y}})/\sqrt{2}$ corresponds to the left- and right-hand circular polarization unit vectors.] For circular polarization, $(u, v) = (1, 0)$ or $(0, 1)$; for elliptic polarization, $0 < u,\ v < 1$. The pulse transmission and reflection are equal to the area ratios of the transmitted and reflected pulses, respectively, to the input pulse. Thus, to compute pulse transmission and reflection numerically, one uses the strategy (i) compute numerically the polarization throughout the bandwidth, and compute the ellipticity to obtain $u(\omega)$ and $v(\omega)$, (ii) for each frequency within the bandwidth, compute $t_\pm$ and $r_\pm$, and (iii) use Eqs. (2) and (3) to compute T and R for both forward and backward directions.

Figure 3(a) plots the polarizations over a frequency range of 10 GHz, assuming the center frequency ω_- corresponds to 1.55 μm wavelength (the lattice constant $a = 0.713\ \mu$m). The polarizations remain essentially circular throughout the entire 10 GHz frequency bandwidth, which corresponds to a pulse with a temporal width $\simeq 0.1$ ns. To investigate the effects of imperfect transmissions at detuned frequencies, we numerically simulated the dynamic process of the propagation of a photon pulse by solving the following set of equations of motion [23]:

$$i\partial_t \phi_R(x, t) = -iv_g \partial_x \phi_R(x, t) + V\delta(x)e_a(t), \tag{4}$$

$$i\partial_t \phi_L(x, t) = +iv_g \partial_x \phi_L(x, t) + V\delta(x)e_a(t), \tag{5}$$

$$i\partial_t e_a(t) = \omega_\pm e_a + V(\phi_R(0, t) + \phi_L(0, t)), \tag{6}$$

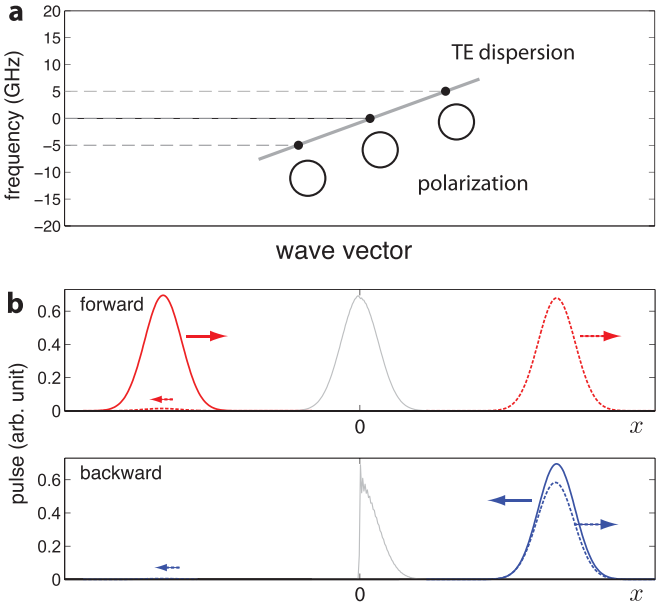

FIG. 3 (color online). Photonic rectification for a pulse with a finite frequency bandwidth. (a) The polarization remains essentially circular throughout a 10 GHz bandwidth, centered at a frequency corresponding to 1.55 μm wavelength. (b) Nonreciprocal pulse propagation in the waveguide at sequential time steps. The transmission in the forward direction is $T_f = 97.6\%$ (upper panel), and is $T_b = 0.7\%$ in the backward direction (lower panel). The input pulse is a 50 ns Gaussian pulse at 1.55 μm wavelength.

where $\phi_R(x,t)$ and $\phi_L(x,t)$ are the wave functions of the right-moving and left-moving photons, respectively, $e_a(t)$ is the quantum dot excitation, V is the waveguide-impurity coupling, v_g is the group velocity of the photon in the waveguide, and $\omega_\pm$ are the transition frequencies for $\Delta m = \pm 1$ transitions. The quantum dot is located at $x = 0$. The above set of the equations of motion already takes into account that the polarizations remain circular throughout the frequency bandwidth of the photon pulse. The general case when the polarization becomes noncircular within the pulse bandwidth can be numerically solved in the same manner and will be presented elsewhere. To solve the equations of motion numerically, we use the pseudospectral method in coordinate space with a nonuniform grid to evolve an initial state specified by $\phi_R(x,0)$, $\phi_L(x,0)$, and $e_a(0)$. The input pulse enters from the left (forward direction) or the right (backward direction); in each case, the quantum dot is initially in the ground state ($e_a(0) = 0$).

The input pulse is a 50 ns Gaussian pulse at 1.55 μm wavelength, which corresponds to a frequency bandwidth $\Delta B = 0.44/(50 \times 10^{-9}) = 8.8 \times 10^{-3}$ GHz $\ll$ 10 GHz. (The rectification function is independent of the pulse shape.) The impurity is an InAs quantum dot located at $x = 0$, with experimental values of radiative lifetime $\tau_r = 2.2$ ns and nonradiative lifetime $\tau_{nr} = 24$ ns, respectively, at 180 K [26]. The external linewidth Γ of the quantum dot due to waveguide-quantum dot coupling is given by $\Gamma = 2\pi/\tau_r = 2.86$ GHz, and the intrinsic dissipation rate of the quantum dot is given by $\gamma = 2\pi/\tau_{nr} = 0.262$ GHz. The angular frequency separation is $\Delta\omega = \omega_+ - \omega_- = 20$ GHz ($\omega_- = 1215.26$ THz and $\omega_+ = 1215.28$ THz at 0.108 T). The Zeeman splitting for this frequency separation is calculated using an effective electron mass of $m_e/2.1$ [27]. Both Γ and $\Delta\omega$ are much larger than the pulse bandwidth. The group velocity v_g can be directly read off from the dispersion diagram of the waveguide; for the photonic line defect waveguide as shown in Fig. 2(b), $v_g = 0.09c$ (c is the speed of light in vacuum) and V is obtained from $\Gamma = V^2/v_g$ [23]. Figure 3(b) plots the nonreciprocal pulse propagation at sequential time steps: The input pulses are indicated by the thick lines, the transmitted and reflected pulses by dashed lines, and the gray lines show the pulse interacting with the quantum dot. In the forward direction, the transmission is $T_f = 97.6\%$ (defined as the area ratio of the transmitted pulse to the input pulse) and $R_f = 2.0\%$ (defined as the area ratio of the reflected pulse to the input pulse), while in the backward direction, the transmission is $T_b = 0.7\%$ and $R_b = 83.9\%$, yielding a contrast $\eta = 0.986$. Note that in the backward direction, the pulse interacts resonantly with the quantum dot, giving rise to a small time delay $\simeq 1.1$ ns, approximately 2.2% of the pulse width. For the case of larger intrinsic dissipation with $\gamma/\Gamma = 0.25$, in the forward operation, we obtained $T_f = 97\%$ and $R_f = 2\%$, while in the backward direction, we obtained $T_b = 4\%$ and $R_b = 64\%$, yielding a contrast of 0.92. The reflected pulse in the backward direction experiences a time delay of 1.1 ns. The time delay stays the same in both cases, as in both cases $\gamma \gg 2\pi\Delta B$ (the pulse bandwidth). For the cases where $2\pi\Delta B \gg \gamma$, the time delay of the reflected pulse would be sensitive to the values of γ. The simulation results indicate that the intrinsic dissipation does not seriously impede the performance of the diode, as in the forward direction the off-resonant pulse interacts weakly with the quantum dot, and thus is insensitive to the dissipation, and in the backward direction the transmission $T_b \simeq (\frac{\gamma}{\gamma+\Gamma})^2$, and the reflection $R_b \simeq (\frac{\Gamma}{\gamma+\Gamma})^2$ for a resonant scattering process [23]. As a result, the contrast is not susceptible to intrinsic dissipation when $\gamma \ll \Gamma$.

The experimental limitation in precisely positioning the quantum dot has been a major obstacle to achieving deterministic photon-quantum dot coupling [28]. The spatial accuracy of placing the quantum dot by electron-beam lithography is $\sim$25 nm, due to imprecision in the electron-beam registration and writing [29]; comparable accuracy has been reported in other photonic systems [30]. We have numerically evaluated the contrast at several sample points which are spatially away from the ideal point with circular polarization [point 2 in Fig. 2(a)], using Eq. (4) [note that in Fig. 2(a) the distance between point 1 and point 2 is 57 nm when $a = 0.714$ μm). At the point 30 nm to the right of point 2, $u \simeq 3.5v$, while at the point 30 nm to the left of point 2, $u \simeq 3.6v$; the contrasts at both points are larger than 0.85, close to that in a periodically poled lithium niobate waveguide [6]. The contrast in fact can be accurately expressed as $\sim(u^2 - v^2)/(u^2 + v^2)$ when $\Gamma \gg \gamma \gg \Delta B$. These results demonstrates the practicality of the proposed device.

As a second example, we consider a 2D holey-cavity waveguide [25]: a dielectric waveguide perforated with a periodic sequence of 12 air holes [Fig. 4(a)]. A resonant cavity mode is introduced by increasing the distance between the two central air holes. The dielectric material is assumed to be Pyrex glass with $\epsilon = 5$. Such a structure has been used as a filter, as the resonant mode gives rise to a transmission peak in the middle of the band gap. Figure 4(b) plots the transmission spectrum for both TE and TM modes. Within the frequency range from 0.275 ($2\pi c/a$) to 0.296 ($2\pi c/a$), only the TE mode exists, and the structure is a SPSM waveguide. At the point in one of the air holes [Fig. 4(a)], the polarization at frequency 0.293 ($2\pi c/a$) is circular [Fig. 4(c)]. The point is located in an air hole so that an impurity can be placed. We have also numerically verified that the polarization remains essentially circular throughout a 10 GHz frequency bandwidth centered at 1.55 μm wavelength.

Finally, we briefly discuss the full three-dimensional realizations. To achieve a full three-dimensional device, we note that if the structure has a mirror symmetry plane at $z = 0$, the eigenmodes within the symmetry plane ($z = 0$)

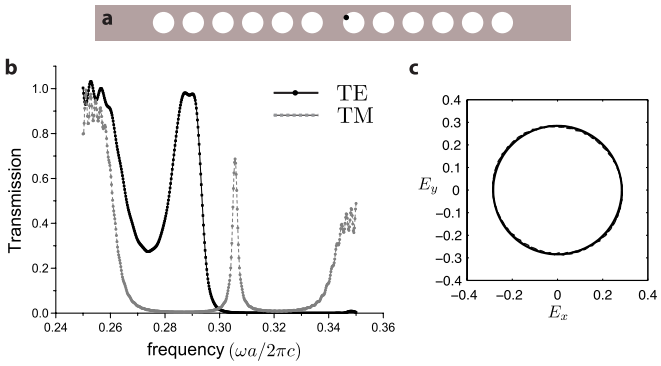

FIG. 4 (color online). Schematics and polarization state of a holey-cavity waveguide. (a) The structure of the holey-cavity waveguide. The width of the waveguide is $1.2a$. The holes have a radius $0.36a$, and are separated by a distance a, except for the two center holes that form the cavity which are separated by a distance $1.4a$. (b) The transmission spectra for both TE and TM modes. (c) The circular polarization at the point shown in (a) at frequency $\omega = 0.293$ $(2\pi c/a)$. Circular polarization exists at three other points via mirror symmetry.

are purely TE and TM polarized [25]; moreover, for thin structures with a mirror symmetry, the modes are essentially TE-like and TM-like, as long as the waveguide thickness is smaller than the wavelength. Alternatively, to emulate the states of the 2D structures, one can sandwich a 3D photonic structure by perfect magnetic conductors [31,32] to obtain the TE states equivalent to the model 2D photonic system. Furthermore, for 3D waveguides that have continuous translational symmetry along the waveguide direction such as fibers, the polarization would remain unchanged along a line parallel to the axis of the waveguide, a feature that could help alleviate the requirement of precise position of the impurity when the waveguides have only discrete translational symmetry. 3D SPSM waveguides with continuous translational symmetry have been demonstrated, for example, by employing the stress-induced birefringence in the core region in optical fibers [33], or by using different sizes of air holes in photonic crystal fibers [34], where the mode degeneracy is broken by lifting the rotational symmetry on the cross section of the waveguide. Through fine-tuning the characteristics such as the stress, or the size and arrangement of air holes, a planar circular polarization may be attained.

This work was supported in part by the Center for Materials Innovation at Washington University in St. Louis (Grant No. 12-2258-94530). J. T. S. acknowledges discussions with C. W. Wong of Columbia University and C. W. Lai of Michigan State University.

*jushen@ese.wustl.edu

[1] M. Soljačić and J. D. Joannopoulos, Nature Mater. **3**, 211 (2004).
[2] P. Michler *et al.*, Science **290**, 2282 (2000).
[3] C. Kurtsiefer, S. Mayer, P. Zarda, and H. Weinfurter, Phys. Rev. Lett. **85**, 290 (2000).
[4] E. Moreau *et al.*, Appl. Phys. Lett. **79**, 2865 (2001).
[5] A. A. Houck *et al.*, Nature (London) **449**, 328 (2007).
[6] K. Gallo, G. Assanto, K. R. Parameswaran, and M. M. Fejer, Appl. Phys. Lett. **79**, 314 (2001).
[7] P. Yeh, *Optical Waves in Layered Media* (John Wiley and Sons, New York, 1988).
[8] B. E. A. Saleh and M. C. Teich, *Fundamentals of Photonics* (John Wiley and Sons, New York, 2007), 2nd ed.
[9] J. Fujita *et al.*, Appl. Phys. Lett. **76**, 2158 (2000).
[10] S. Mujumdar and H. Ramachandran, Opt. Lett. **26**, 929 (2001).
[11] M. Scalora, J. P. Dowling, C. M. Bowden, and M. J. Bloemer, J. Appl. Phys. **76**, 2023 (1994).
[12] T. Yoshie *et al.*, Nature (London) **432**, 200 (2004).
[13] H. de Riedmatten *et al.*, Nature (London) **456**, 773 (2008).
[14] K. K. Y. Lee, Y. Avniel, and S. G. Johnson, Opt. Express **16**, 15 170 (2008).
[15] W. Hansen *et al.*, Phys. Rev. Lett. **62**, 2168 (1989).
[16] R. Rinaldi *et al.*, Phys. Rev. Lett. **77**, 342 (1996).
[17] R. Hanson *et al.*, Phys. Rev. Lett. **91**, 196802 (2003).
[18] W. S. Boyle, J. Phys. Chem. Solids **8**, 321 (1959).
[19] P. Fisher and H. Y. Fan, Phys. Rev. Lett. **2**, 456 (1959).
[20] S. Zwerdling, K. J. Button, and B. Lax, Phys. Rev. **118**, 975 (1960).
[21] K. Seeger, *Semiconductor Physics* (Springer-Verlag, Berlin, 2004), 9th ed.
[22] R. W. Boyd, *Nonlinear Optics* (Academic, New York, 2008), 3rd ed.
[23] J. T. Shen and S. Fan, Opt. Lett. **30**, 2001 (2005).
[24] E. Waks and J. Vuckovic, Phys. Rev. Lett. **96**, 153601 (2006).
[25] J. D. Joannopoulos, S. G. Johnson, J. N. Winn, and R. D. Meade, *Photonic Crystals: Molding the Flow of Light* (Princeton University Press, Princeton, NJ, 2008), 2nd ed.
[26] E. Harbord, P. Spencer, E. Clarke, and R. Murray, Phys. Rev. B **80**, 195312 (2009).
[27] T. Mensing *et al.*, Appl. Phys. Lett. **82**, 2799 (2003).
[28] A. Badolato *et al.*, Science **308**, 1158 (2005).
[29] Chee Wei Wong (private communication).
[30] A. Dousse *et al.*, Appl. Phys. Lett. **94**, 121102 (2009); S. M. Thon *et al.*, *ibid.* **94**, 111115 (2009); T. van der Sar *et al.*, *ibid.* **98**, 193103 (2011).
[31] A. P. Feresidis, G. Goussetis, S. Wang, and J. C. Vardaxoglou, IEEE Trans. Antennas Propag. **53**, 209 (2005).
[32] I. Lindell and A. Sihvola, J. Electromagn. Waves Appl. **19**, 861 (2005).
[33] W. Eickhoff, Opt. Lett. **7**, 629 (1982).
[34] K. Saitoh and M. Koshiba, IEEE Photonics Technol. Lett. **15**, 1384 (2003).